[6] Steinauer, J., "Similar Solutions for the Laminar Wall Jet in a Decelerating Outer Flow," *AIAA Journal*, Vol. 6, No. 11, Nov. 1968, pp. 2198–2200.

[7] Rogers, D., "Reverse Flow Solutions for Compressible Laminar Boundary Layer Equations," *The Physics of Fluids*, Vol. 12, 1969, pp. 517–523.

[8] Rosenhead, L., *Laminar Boundary Layers*, Chap. V, pp. 245–252.

[9] Libby, P. A. and Liu, T. M., "Further Solutions of the Falkner-Skan Equation," *AIAA Journal*, Vol. 5, No. 5, May 1967, pp. 1040–1042.

Magneto-Hypersonic Boundary-Layer Interactions

M. S. Sastry* and S. Chandran†
Space Science and Technology Centre, Trivandrum, India

Nomenclature

B_0 = applied transverse magnetic field
L = characteristic length = $M_1^2\mu\omega/\rho_1 u_1$
M = Mach number
m = $2(1 - \text{Log } 2)/(\gamma - 1)$; γ = specific heats ratio[3]
P^* = pressure ratio = P_2/P_1
u = x component of velocity; x being the surface coordinate
σ = electrical conductivity
ρ = density
ξ = x/L
η = δ/L
δ = boundary-layer thickness
μ = viscosity coefficient
REX = $\rho_1 u_1 x/\mu_1$

Subscripts

1 = $x = +\infty$ on the boundary-layer surface
2 = $x = x$ on the boundary-layer surface
ω = surface of the plate

In Ref. 1 to study the magneto-hypersonic viscous interactions for the insulated flat plate, the hydromagnetic compressible boundary-layer equations of Meyer[2] for the case of no induced magnetic field were investigated by a generalized von Kármán Integral method. Corresponding to the nonmagnetic momentum integral equation of Pai[3] the magnetic equation can be derived and the additional term involved is obtained as $-(\sigma B_0^2 M_2^2 L/2\rho_2 u_2)(P^*\eta)$. Since the fluid characteristics involving the subscript 2, in an interaction phenomena are unknown, an approximation made in Ref. 1 was that $(M_2^2/\rho_2 u_2) \approx (M_1^2/\rho_1 u_1)$ which then converts the unknown magnetic parameter into the square of the Hartmann number, in terms of the characteristics with subscript 1, which are known.[3] But this approximation, which implies that $P^* = 1$ made the analysis of Ref. 1 valid for the weak interaction case only. In fact, it can be seen from the present analysis that no such approximation is needed for discussing the magneto viscous interactions of the hypersonic boundary layer flow. Following Ref. 3 the magnetic momentum integral equation under the hypersonic conditions can be derived as,

$$(2/m) = d/d\xi(\eta^2 P^*) - (\sigma B_0^2 L/m)(M_2^2/\rho_2 u_2)(\eta^2 P^*) \quad (1)$$

Received May 27, 1969; revision received September 12, 1969.

* Scientific Officer, Applied Mathematics Division; formerly Engineer.
† Engineer, Aerodynamics Division.

Since $u_2/u_1 \backsim 1$ for the hypersonic case,

$$(M_2^2/\rho_2 u_2) = (u_2/\gamma P_2) = u_1(u_2/u_1)/\gamma P_1(P_2/P_1) \approx (u_1/\gamma P_1)(1/P^*) = (M_1^2/\rho_1 u_1)(1/P^*)$$

So that Eq. (1) becomes

$$(2/m) = d/d\xi(\eta^2 P^*) - (\sigma B_0^2 L/m)(M_1^2/\rho_1 u_1)(\eta^2) \quad (2)$$

But

$$(\sigma B_0^2 L . M_1^2/\rho_1 u_1) = (\sigma B_0^2 L^2/\mu\omega) = H_m^2$$

Where H_m is the Hartmann number and hence Eq. (2) simplifies to

$$(2/m) = d/d\xi(\eta^2 P^*) - (H_m^2/m)\eta^2 \quad (3)$$

Equation (3), being independent of the approximation of Ref. 1, is valid for both strong and weak interaction cases and can be solved for the corresponding cases by using the corresponding pressure distributions.

For the strong case, P^* can be taken as,

$$P^* = \{\gamma(\gamma + 1)M_1^2/2\}(d\eta/d\xi)^2 \quad (4)$$

Substituting relation (4) in Eq. (3) and observing as in Ref. 3 that near the origin,

$$\eta \cong (32/9mc)^{1/4}\xi^{3/4} \quad (5)$$

Where $c = \gamma(\gamma + 1)M_1^2/2$, a series solution for η may be written as

$$\eta = \zeta^3 \sum_0^\infty b_m \zeta^m \quad (6)$$

where $\zeta = \xi^{1/4}$ and the rest is as in Ref. 3.

For the weak case, if it is assumed that $P^* = 1$ can be put in (3) then a simple solution can be obtained as

$$\eta^2 = \{e^{(H_m^2/m)\xi} - 1\}(2/H_m^2) \quad (7)$$

which for small ξ implies that $\eta \propto \xi^{1/2}$, which may as well mean that there is no viscous interaction at all. Similarly if $P^* = 1$ used in (7) be replaced by $P^* = 1 + \gamma M_1 d\eta/d\xi$ then the analysis of Eq. (3) will show that $\eta \propto \xi^{2/3}$. Hence,

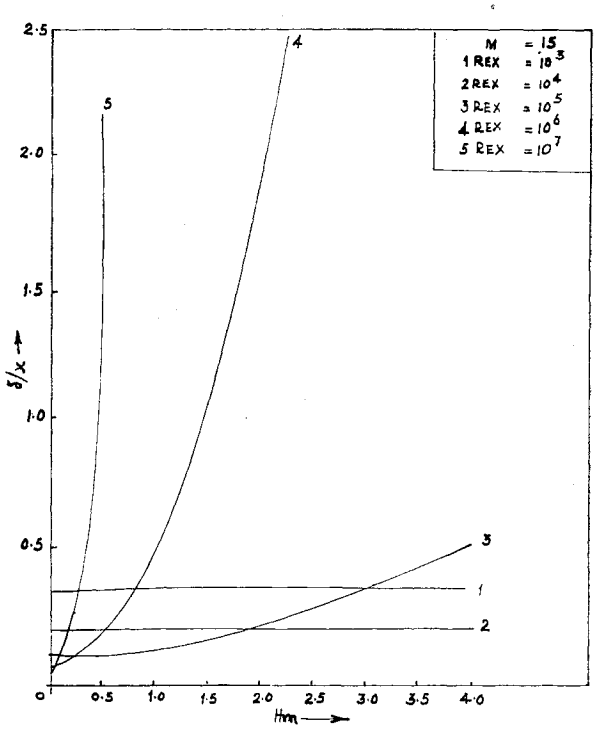

Fig. 1 Boundary-layer thickness and Hartmann number.

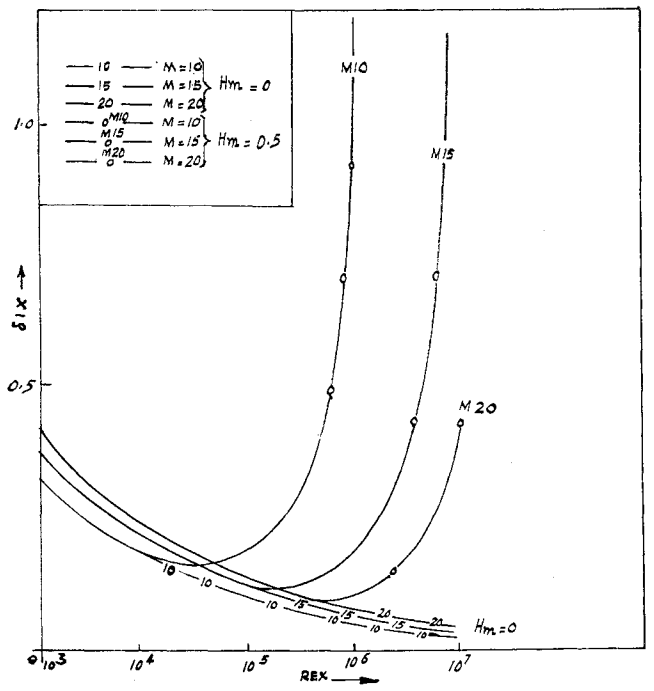

Fig. 2 Boundary-layer thickness and Reynolds number.

$P^* = 1 + \gamma M_1 d\eta/d\xi$ can be assumed to be the pressure distribution for the transition zone from strong to the weak case, so that the boundary layer thickness can be seen to proportionally vary gradually from $\xi^{3/4}$ to $\xi^{2/3}$ and then to $\xi^{1/2}$. This type of analysis gives us a complete flow picture of the magneto viscous boundary-layer interactions and this was made possible because Eq. (3) is derived to be valid for all cases unlike Ref. 1, where a similar equation of the type of Eq. 3 was valid only to the weak case, due to the approximations made therein.

The graph in Fig. 1 illustrates the behavior of δ/x with respect to Hartmann number for various local Reynolds number and the graph in Fig. 2 illustrates the behavior of δ/x with respect to local Reynolds numbers for $H_m = 0$ and $H_m = 0.5$ and for different Mach numbers. Though, the qualitative behaviour in this strong case also is the same as that of Ref. 1 yet quantitatively it is interesting to see that δ/x is being dominated by the magnetic effects for $M_1 = 10$ from $REX > 10^4$ onwards itself unlike Ref. 1, where the magnetic effects are seen appreciably only after $REX > 10^5$. The dominance of the magnetic fields after $REX > 10^4$ in comparison to Ref. 1 may be perhaps due to the reason that at these Reynolds numbers, the viscous interactions are not really strong and the dominance is obviously because, the strong viscous effects similar to Ref. 1 die out at these high Reynolds numbers. There are no magnetic effects for $REX \leq 10^4$.

In Fig. 1 and Fig. 2 the graphs of Ref. 1 are not drawn for the comparison purposes, since in the light of the present analysis the results of Ref. 1 can be taken to be valid for either a weak case or a transition case and the present results are exclusively for the strong case. Naturally δ/x for the same H_m, REX, and M_1 is higher than that of Ref. 1.

References

[1] Sastry, M. S., "Magneto Hypersonic Boundary-Layer Flow past a Plate," *AIAA Journal*, Vol. 5, No. 1, Jan. 1967, pp. 167–168.

[2] Meyer, R. C., "On Reducing Aerodynamic Heat Transfer Rates by Magnetohydro-Dynamic Techniques," *Journal of the Aerospace Sciences*, Vol. 25, 1958, pp. 561–566.

[3] Pai, S. I., "Hypersonic Viscous Flow Over an Insulated Wedge of an Angle of Attack," Rept. B.N. 42, Univ. of Maryland; also Rept. OSR-TN-54-321 Oct. 1954, Air Research and Development Command, Office of the Scientific Research.

Electron Density Measurements ahead of Shock Waves in Air

MASAYUKI OMURA* AND LEROY L. PRESLEY*
NASA Ames Research Center, Moffet Field, Calif.

THE existence of free electrons ahead of shock waves associated with high-speed bodies entering the earth's atmosphere has been ascertained from observation of both man-made entry bodies and meteors. Several laboratory studies directed toward understanding the production of precursor electrons have been conducted in diaphragm-type shock tubes.[1–3] For these studies argon was used as a working gas and the shock velocities were below 8.7 km/sec. This Note describes recent measurements of precursor electron densities in pure nitrogen and in air at shock velocities between 9.8 and 13.2 km/sec.

The experimental observations were made in a 30.48-cm-diam arc driven shock tube described in Ref. 4. The measurements were made about 13 m downstream of the diaphragm, using an 8.5 GHz microwave interferometer for the diagnostics. No significant modifications were made to the well established technique of using theoretical expressions to relate the experimentally observed phase shift of the microwave signal transmitted across the shock tube to the electron density.[5] Collimation lenses, located in both the transmitting and receiving horns were protected from the hot test gas by half-wave plates made of lucite. The interferometer has a range of sensitivity from about 10^9 to 10^{12} electrons/cm^3.

Typical electron density profiles for various shock velocities in air at an initial pressure of 0.2 torr are shown in Fig. 1. The most significant results presented in Fig. 1 are the high electron densities, in excess of 10^{10} cm^{-3} at distances greater than 5 m ahead of the higher velocity shock waves, and the large dependence of the data upon the shock wave velocity.

The high electron densities that are observed raise questions regarding the source of the electrons as well as dependency of the data upon the particular shock-tube testing technique that was used. The source of precursor electrons is widely accepted to be photoionization of the gas ahead of the shock wave. A qualitative determination of the dependency of electron production upon photoionization of the gas was obtained by placing a plastic film, which covered the entire shock-tube cross section, between the test section and the oncoming shock wave. This film, which absorbed all radiation at wavelengths shorter than 2600 Å, completely suppressed all measurable electron production in the test section. Since diffusion of electrons ahead of the shock wave is confined to very small distances, the role of radiation at wavelengths shorter than 2600 Å, i.e., ultraviolet radiation, was

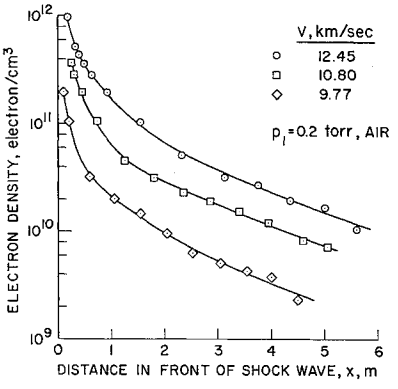

Fig. 1 Typical electron density profiles in air.

Received August 18, 1969.

* Research Scientist